Supplemental Information

A 4 Hz Oscillation Adaptively Synchronizes

Prefrontal, VTA, and Hippocampal Activities

Shigeyoshi Fujisawa and György Buzsáki

SUPPLEMENTAL FIGURES
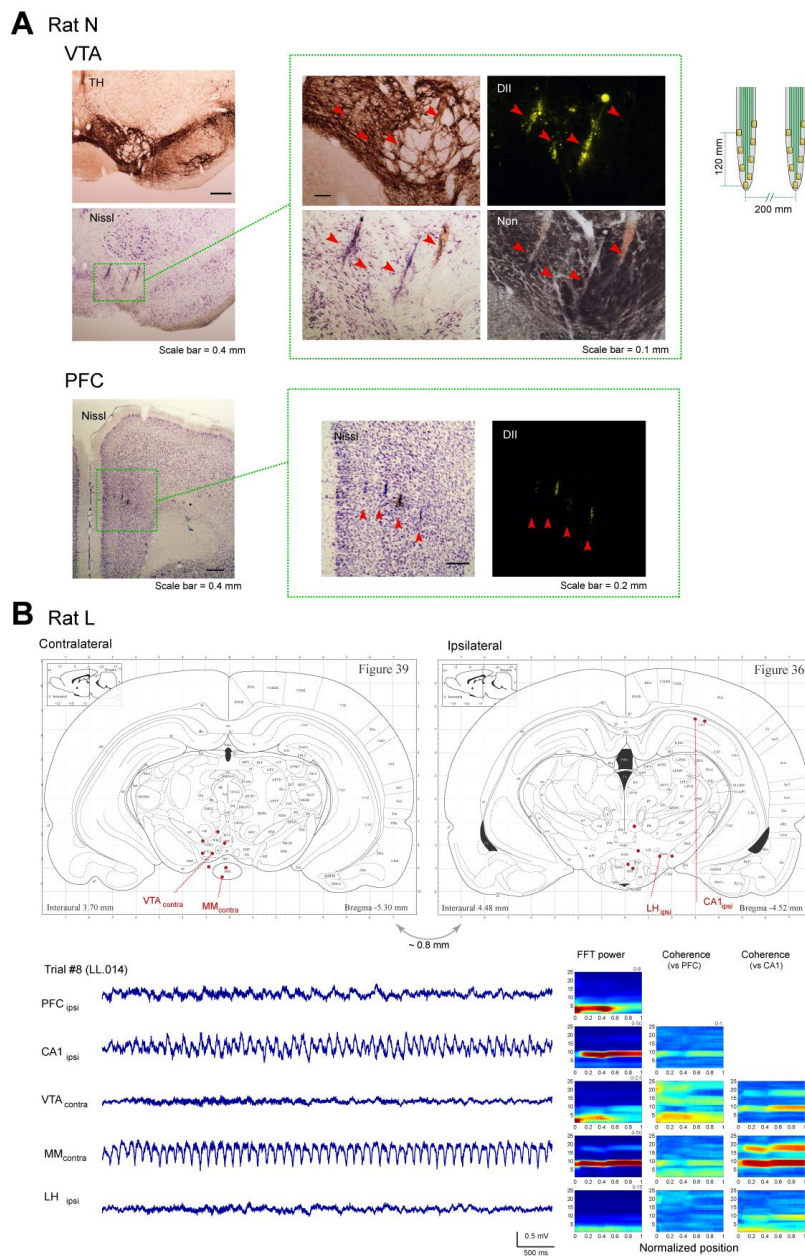
Figure S1.

(A) Silicon probe recording sites in VTA and PFC of rat N. Arrowheads, DiI-labeled tracks superimposed on Nissl-stained, tyrosine hydroxylase immunostained (TH) or native, non-stained (Non) sections. A small amount of DiI was applied on the back side of silicon probes before implantation.

(B) Wire tetrode recording sites and corresponding electrical patterns in Rat L. In this animal, an array of the recording tetrodes was positioned in medial mammillary nucleus (MM), lateral hypothalamic area (LH) and VTA. Despite the spatial proximity of MM, LH and VTA (~1mm), the LFPs of these structures were characteristically different. MM LFP showed strong theta oscillation during maze running, which was strongly coherent to CA1 theta (coherence ~1; Kirk et al. 1996). In contrast, VTA activity was characterized by 4-Hz oscillation, coherent with PFC activity. LH LFP showed neither 4-Hz nor theta frequency oscillations. Stereotaxic coordinates are from Paxinos and Watson (1998).
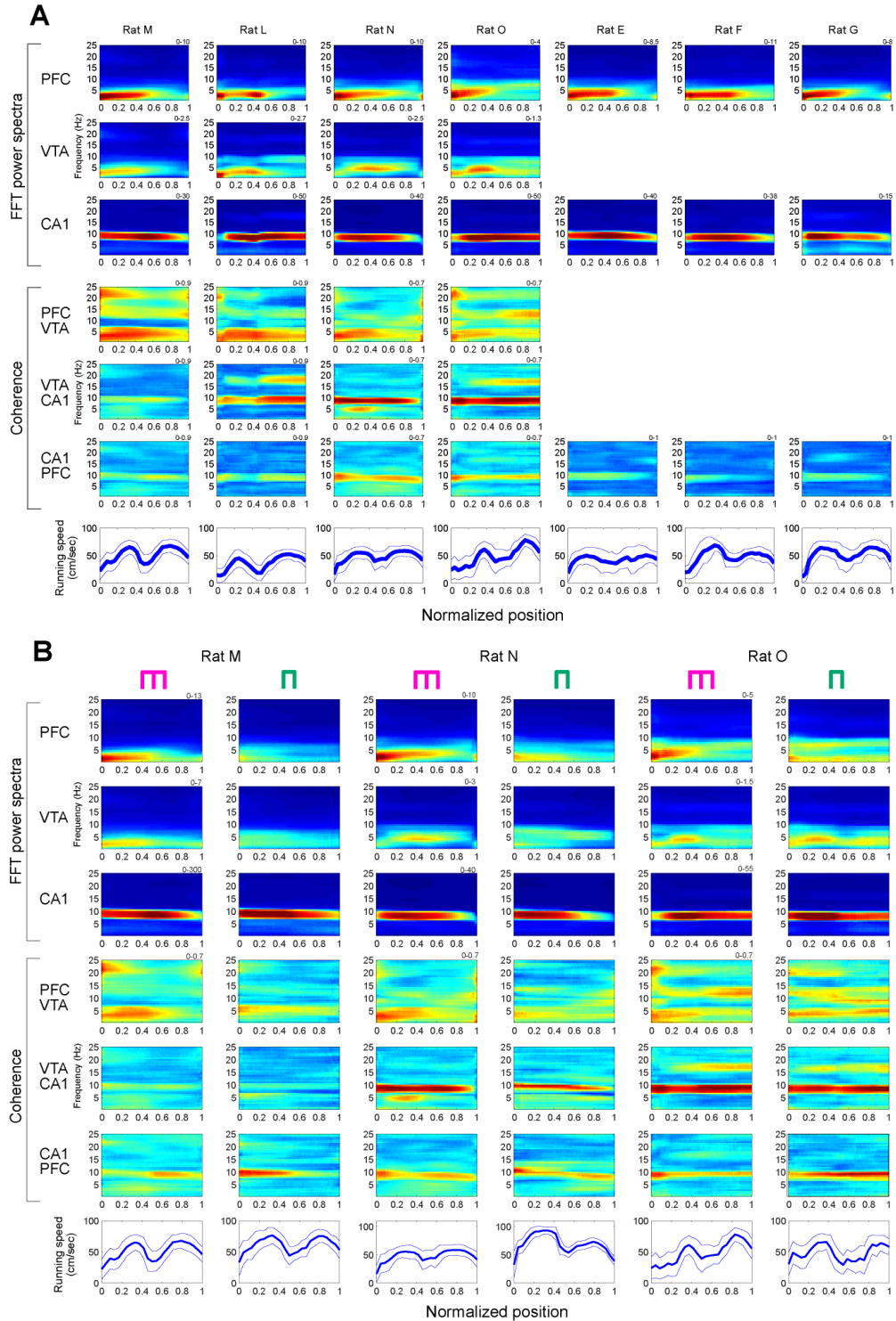
Figure S2. (A) Time-resolved power (PFC, VTA and CA1) and coherence spectra as the function of position in the maze, for each rat. In rats M, N, L and O triple-region recordings were made in PFC, VTA and the hippocampal CA1 pyramidal layer. In rats E, F and G simultaneous recordings were obtained from PFC and CA1. Bottom, running speed (mean±SD). Compare with Figure 1C. Note that PFC and VTA 4-Hz power and their coherence were consistently high in the central arm of the maze. Theta power and coherence between hippocampus and PFC were variable across rats. **(B)** Time-resolved power (PFC, VTA and CA1) and coherence spectra as the function of position in the maze during the working memory task (left columns) and control task (right columns). These two tasks were performed in the same days. Bottom, running speed (mean±SD). Compare with Figure 1C, F.
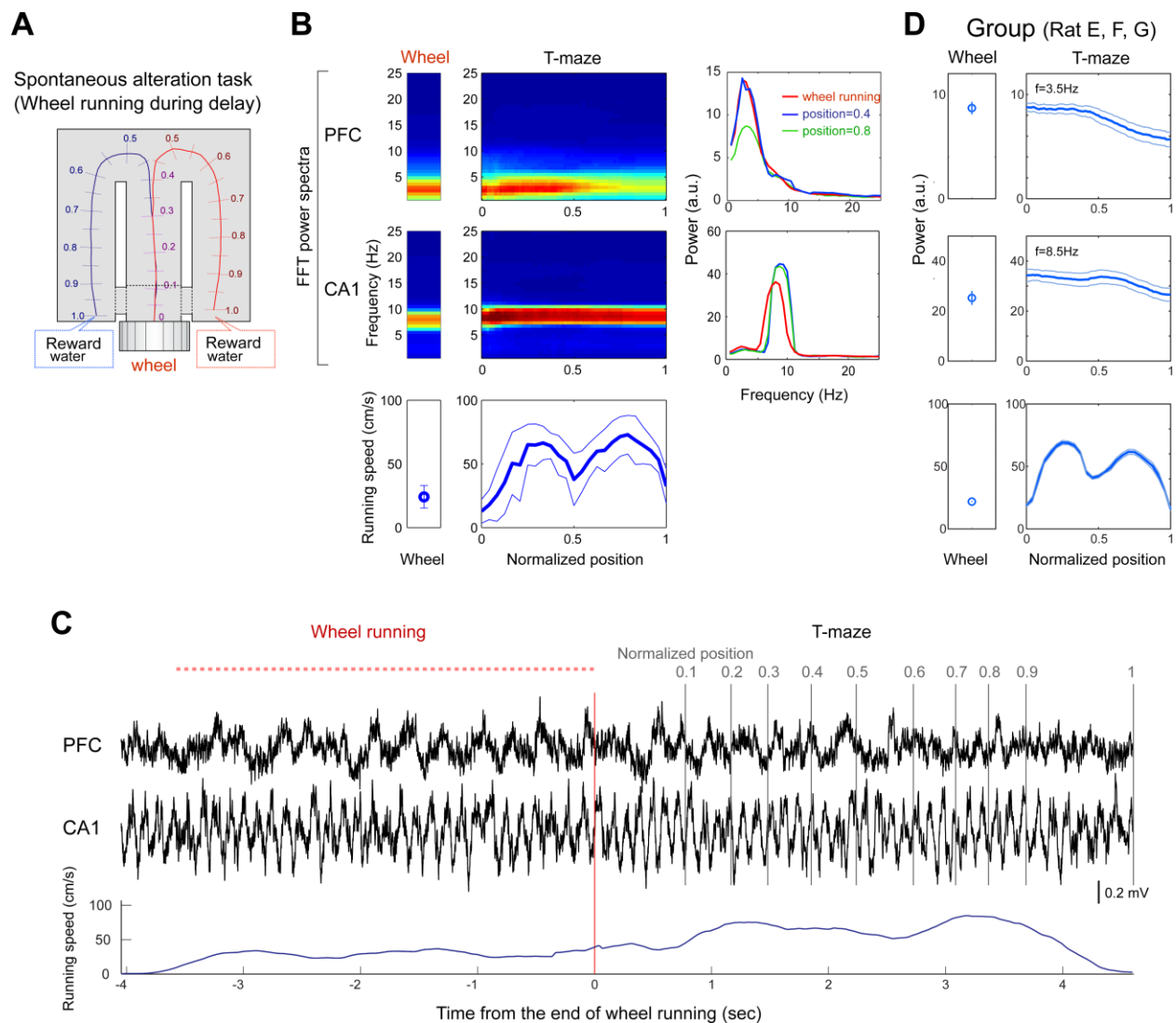
Figure S3. Enhanced and sustained power of 4-Hz rhythm in PFC was also observed during a spontaneous alteration task with delay. **(A)** Three animals (E, F and G) were trained to perform a spontaneous alteration task. During the delay period, the animal was required to run in the wheel for at least 3 sec (Pastalkova et al., 2008). A water drop was given as the reward at the end of the left and right arms. **(B)** Time-resolved power spectra for rat E, as the function of position. Note enhanced 4-Hz power in PFC during both wheel running and in the central arm, i.e., when working memory is required. **(C)** Representative LFP traces from PFC and CA1 sites in a single trial. **(D)** Mean (±SEM) power of 4-Hz and theta oscillations for three rats. Note dissociation between running speed and 4-Hz power in the wheel, central and side arms of the maze.
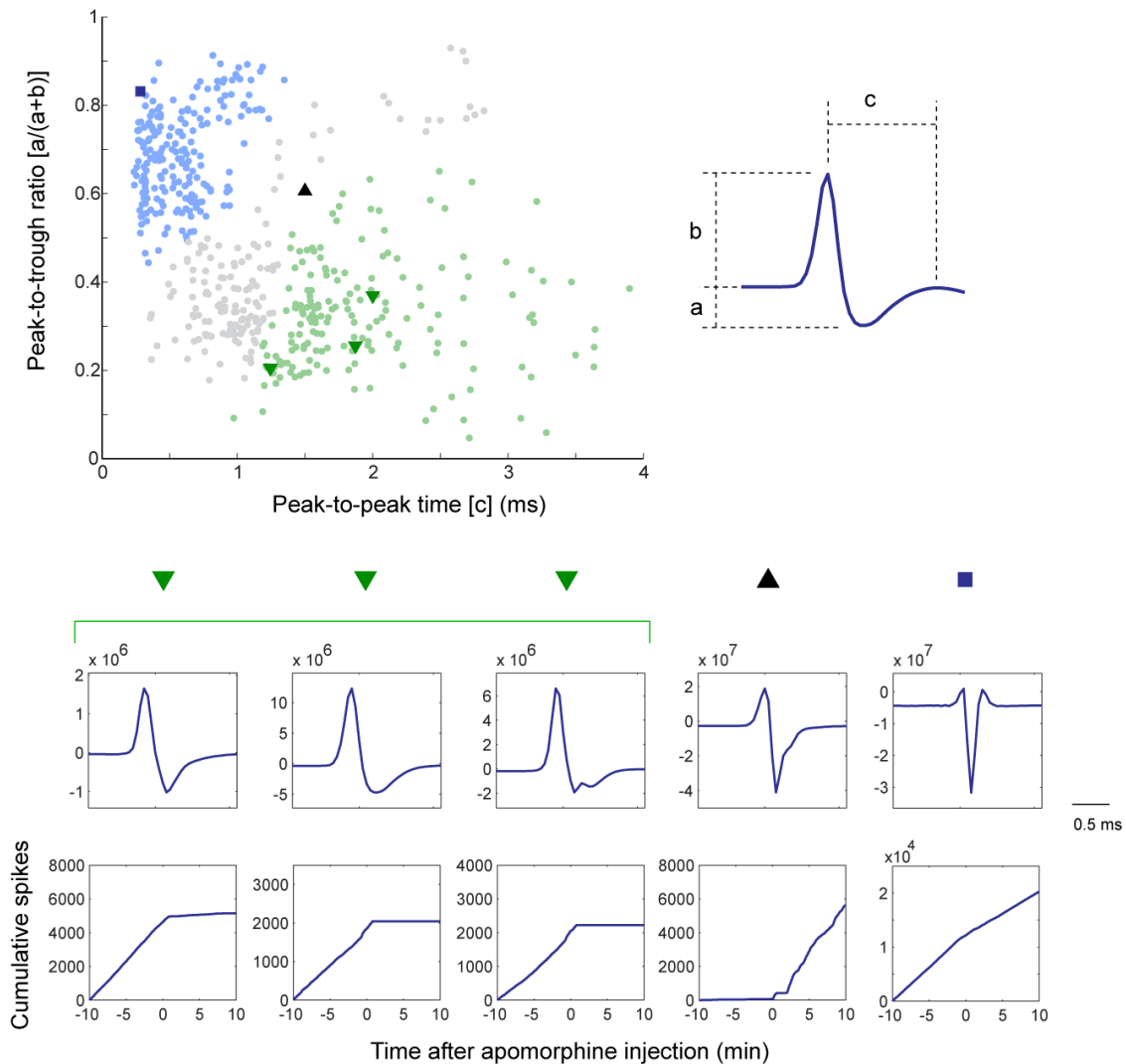
Figure S4. Classification of VTA neurons. (Top) 2-D plot of peak-to-trough ratio and peak-to-peak time (see right) of spike waveforms (1 Hz - 5 kHz). Green and blue dots indicate putative dopaminergic and GABAergic neurons conjectured by their wave shapes. (Bottom) Waveform and response to apomorphine injection (at time 0, i.p., 2.5mg/kg) of 5 neurons from rat O. Green triangle, neurons with wide spike waveform were strongly inhibited (left three neurons) by apomorphine injection, indicating that these neurons are likely dopaminergic (Robinson et al., 2004; Roesch et al., 2007; Jin and Costa, 2010). The neuron marked by the blue rectangle had a narrow spike wave shape and was not affected by apomorphine injection, indicating that this neuron is GABAergic (Roesch et al., 2007; Jin and Costa, 2010). The neuron with the black triangle represents an 'unclassified' cell. Unclassified neurons (gray dots) were not included in the analyses.

A Rat-N all VTA units

First NP in   Last NP out

Nose-poking-selective

Maze-selective

Other (uniform)
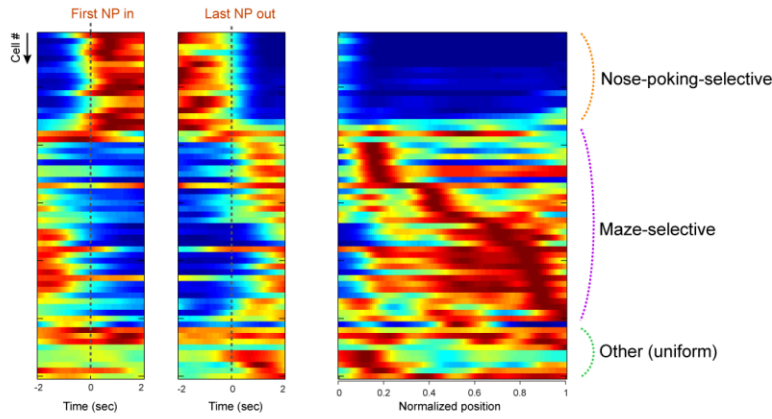
B Nose-poking-selective cell
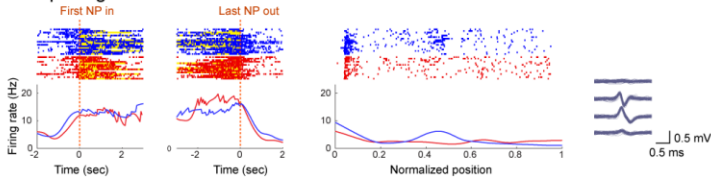
Maze-selective cell
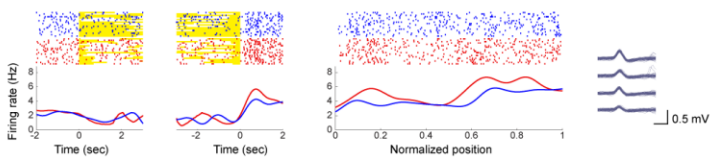
Maze-selective cell (rhythmic)
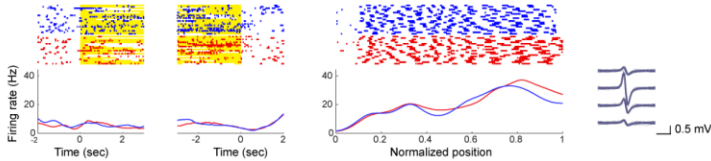
Nose-poking-and-maze-selective cell
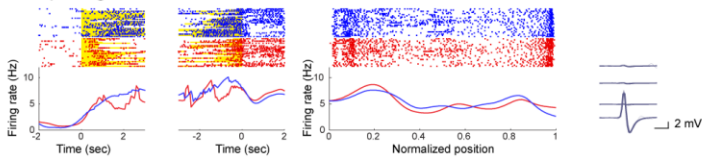
Other
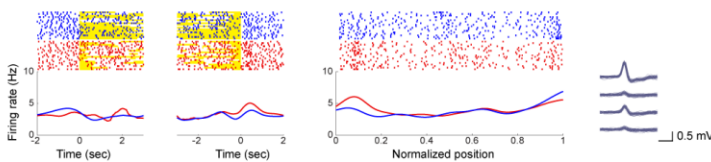
Figure S5. Behavior-related firing patterns of VTA neurons in the working memory task. Using the simplest categorization, we identified three behavioral correlates of firing patterns in VTA neurons. Nose-poking-selective cells were either active during nose-poking (NP) periods or suppressed their activity. Neurons with increased firing activity might be related to reward expectation, described earlier in Pavlovian conditioning paradigms (Waelti et al., 2001; Schultz 2006; Roesch et al., 2007). Maze-active neuron increased their rates at some aspects of maze running. Some of these neurons fired rhythmically with peaks at 2-5 Hz in their phase-histograms. Neuron in the 'Other' category did not show selectivity in any phase of the task. **(A)** VTA neurons grouped by the 3 categories. **(B)** Examples of neurons in each category. The third and fourth neurons are also shown in Fig 4D. VTA neurons show a rich diversity of firing patterns (Puryear et al., 2010), which may be related to their wide-range innervations by multiple structures. While cortical afferents, along with projections from the bed nucleus of the stria terminalis, and laterodorsal and pedunculopontine tegmental nuclei represent the bulk of VTA-bound projections, large numbers of nuclei, which form a nearly continuous formation extending from the prefrontal cortex to the caudal brainstem, provide sparse, mostly glutamatergic afferents (Geisler and Zahm, 2005; Geisler et al., 2007). Of the putative dopaminergic neurons in VTA, only 5.4% were classified as goal-predictive (P<0.05).
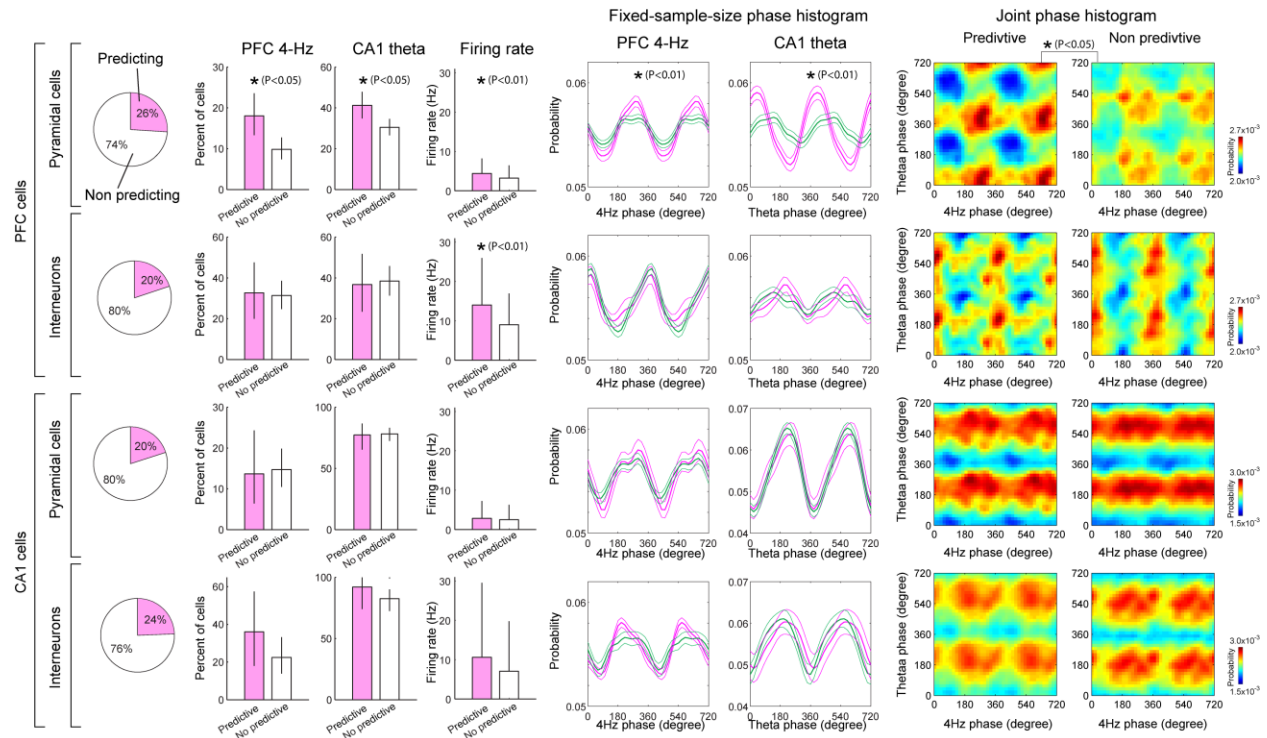
Figure S6. Trial outcome-predicting PFC neurons are more strongly modulated by the 4-Hz oscillation than non-predicting cells. **(A)** Pie charts, fraction of goal-predicting (pink; significantly different mean discharge rates at position 0-0.3 in left and right trials; permutation test; P<0.05) and non-predicting (white) neurons. Graphs, percent of neurons significantly phase-locked (P<0.05; Rayleigh test) to 4-Hz or theta oscillations. Bars, Clopper-Pearson confidence intervals (P < 0.05). **(B)** Firing rates (mean ± SD) of the goal-predicting (pink) and non-predicting (light green) neurons of PFC and CA1, in the central arm (P<0.01; t-test). **(C)** Mean phase histograms of the goal-predicting (pink) and non-predicting (light green) neurons of PFC and CA1. Peak-to-trough height of the phase histogram was used for statistical comparison (permutation test; P< 0.05). In order to rule out the possibility that the difference of phase-modulation between the prediction and non-predicting neurons are simply due to the firing-rate difference between them, we used fixed-sample size method (Vinck et al., 2010). First, we chose the neurons whose firing rates are more than 1 Hz in the central arm for this analysis, in order to remove neurons which did not fire in the central arm. With this criterion, the minimum spike count of all single neurons in the central arm was 46 counts. Then, to reduce a bias by sampling numbers, we compute phase histograms using the fixed sample number (=46) for all neurons. To use all available data for neurons whose spike counts are more than 46, a bootstrap without replacement (i.e. every observation can enter one bootstrapped sample only once) was used to reduce the variance of the new estimate (Vinck et al., 2010). This fixed-sample size analysis revealed that the differences of phase-modulation by 4-Hz and theta oscillations between prediction and non-predicting neurons were still significant. **(D)** Mean joint phase histogram of the goal-predicting and non-predicting neurons. Peak-to-trough height of the joint phase histogram was used for the assessment of statistical significance (permutation test; P< 0.05).
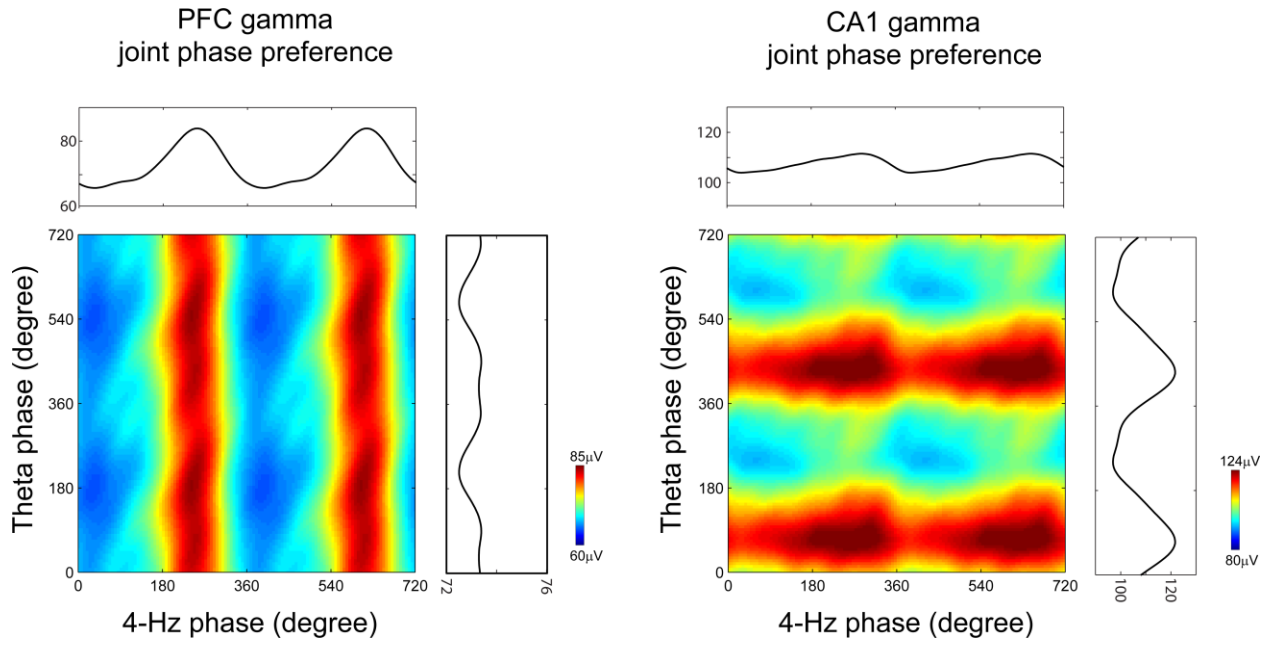
Figure S7. Joint 4-Hz and theta phase preference of gamma amplitude in PFC (left) and CA1 (right). Although gamma amplitude is co-modulated by both oscillations, PFC gamma waves are more strongly affected by the 4-Hz rhythm, whereas CA1 gamma waves are phase-locked mainly to theta oscillation.
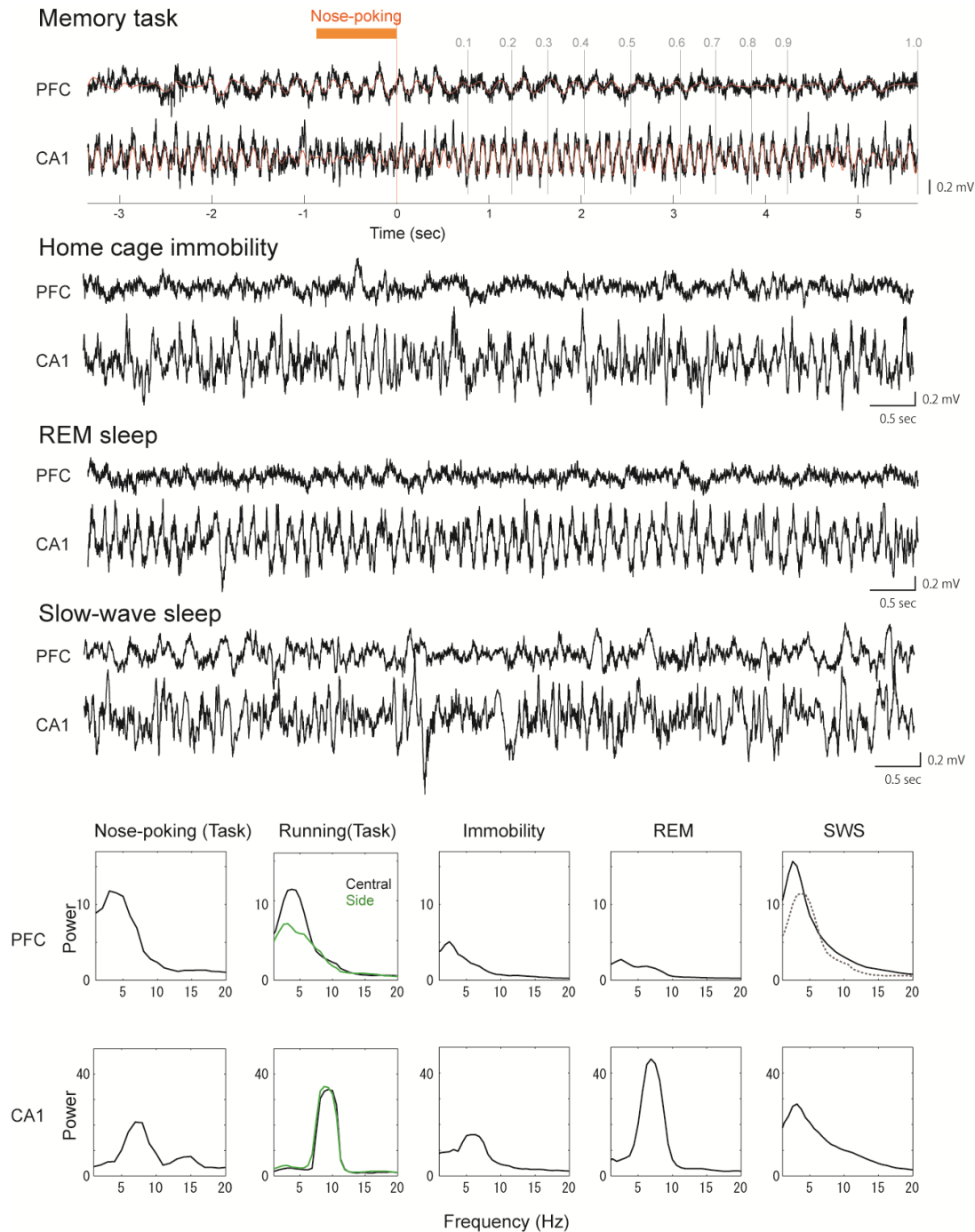
Figure S8. LFP patterns in various brain states.

Representative LFP traces and power spectra during nose-poking and maze running in the memory task, immobility in the home, REM and slow-wave sleep (SWS). Power of 4-Hz oscillation was high during nose-posing and running in the central arm, but low during immobility and REM sleep in the home cage. In SWS, with a large peak ~2Hz is present. The peak at 2 Hz in both PFC and hippocampus is a reflection of slow oscillation, the main characteristics of non-REM sleep (Steriade et al., 1993; Isomura et al. 2006). For comparison, the spectrum during running in the central arm is superimposed (dotted line). The high power of hippocampal theta and the lowest power of 4-Hz oscillation during REM sleep and the high power of PFC 4-Hz and the relatively low hippocampal theta power during nose poking illustrate that the two rhythms are generated by different mechanisms. Spectra were calculated from all trials of a single session from rat E.

SUPPLEMENTAL METHODS

Behavioral training methods

Working memory task. Seven adult male (3-5 months old) rats (Rat E, F, G, L, M, N and O) were trained in an odor-based delayed matching-to-sample task prior to surgery (Fujisawa et al., 2008). The training apparatus was a modified figure-8 T-maze with a start area where the sample odors (chocolate or cheese) were presented and goal arms, which contained the reward. After consumption of the reward the rats could freely return to the start arm and initiate a new trial (Fig 1A). The animals were required to nose-poke into a hole in the start box and the odor cue was given. If the cue was cheese odor, a piece of cheese (300mg) was given at the end of the right arm as reward. If the cue was chocolate, the reward was a piece of chocolate (300mg) at the left. Because the reward was placed in the goal arm prior to the trial initiation by the rat, its odor could serve, in principle, as an undesirable spatial cue. To control for this, pieces of both rewards were set in both arms. However, while the correct reward was accessible, the other ("odorant distractor") was covered with a meshed metal bowl to prevent rat from accessing it. In the home-cage, access to food was not restricted, though water was withheld for 12 hours for the purpose of controlling appetite for food. The rats were given water before the working-memory-task session until they were fully satisfied. The reward types in the side arms varied across rats. Rats were trained in 2 stages. For 10 days, they were pre-trained in a small T-maze (with stem length of 30cm). After pre-training, they were retrained in the figure-8 T-maze (Fig. 1B). Rats learned this task with ~85% accuracy within approximately 10 days. Seven rats with a performance better than 85% correct choices in 5 consecutive days were chosen for surgery. In the recording sessions, the mean correct performance was 92.7%. For recording LFP and neuronal spikes, rats were implanted with silicon probes or tetrodes in the PFC, hippocampus CA1, and VTA (PFC-CA1 double recordings in 3 rats, PFC-VTA-CA1 triple recording in 4 rats; Fig. 1B; Supplementary Fig. 1).

Non-memory control task. Three out of the 7 seven rats (Rat M, N and O) were also trained in a control, non-memory task. The left arm of the maze was blocked at the choice point, so that the animals could only enter the right arm and were always rewarded with a drop of water. To initiate a trial in the control task, the rats were required to nose-poke while coconut odor as presented. The control (non-memory) task was performed after the working memory task and a 1~2 hour rest period in the home cage.

Delayed spontaneous alternation task. Three out of the 7 seven rats (Rat E, F and G) were trained in a delayed spontaneous alteration task. The running wheel (10 cm wide, 29.5 cm diameter) was attached to a wall of the delay area (Supplementary Fig. 3A). The animal was required to run in the wheel for at least 3 sec during the delay periods (Pastalkova et al., 2008), in order to examine the relationship between theta and 4-Hz activities in the delay periods. A water drop was given as a reward at the end of the left and right arms. The delayed spontaneous alteration task was performed after the working memory task and a 1~2 hour rest period

in the home cage.

Surgery and recording

General surgical procedures for chronic recordings have been described elsewhere (Fujisawa, et al., 2008). In short, 3 rats were implanted with silicon probes in the prefrontal cortex (AP=3.0-4.4 mm, ML=0.5 mm, DV=2.0-3.5mm) and CA1 pyramidal cell layer (AP=-6.3mm, ML=5mm, DV=3.6mm) (Rat E, F and G), and 4 rats were implanted with silicon probes and/or tetrodes in PFC (AP=3.0 mm, ML=0.5 mm, DV=2.0-3.5mm), CA1 (AP=-5.3mm, ML=3-4 mm) and VTA (AP=-5.3mm, ML=1mm, DV=8.5mm, bilaterally for 3 rats) (Rat L, M, N and O; Supplementary Fig 1). The recording silicon probe or tetrodes was attached to a micromanipulator and moved gradually to its desired depth position. The probe consisted of 4 or 8 shanks (200-µm shank separation) and each shank had 8 recording sites (160 μm^2 each site; 1-3 MΩ impedance), staggered to provide a two-dimensional arrangement (20 µm vertical separation; Supplementary Fig. 1). In all experiments ground and reference screws were implanted in the bone above the cerebellum. During the recording sessions, neurophysiological signals were acquired continuously at 20 kHz and passband filtered (1Hz to 5kHz) on a 128-channel DataMax system (16-bit resolution; RC Electronics). The wide-band signal was downsampled to 1.25 kHz and used as the local field potential (LFP) signal. For tracking the position of the animals on the task track, two small light-emitted diodes (5-cm separation), mounted above the headstage, were recorded by a digital video camera and sampled (at 40 Hz). Spike sorting was performed semi-automatically, using KlustaKwik (available at: http://osiris.rutgers.edu/BuzsakiHP/Downloads/downloads.html), followed by manual adjustment of the clusters. Data recorded from PFC of 3 of the seven rats in the present study has been reported earlier (Fujisawa et al., 2008).

Histological localization of recording sites

Because of the small volume of the silicon probe shank and its sharp profile, the track of the shanks can be rarely found in histological sections even several weeks after implantation. To facilitate track identification, the back of the shanks was painted with DiI prior to implantation. To identify the depth location of a specific recording site, a small current (2 µA for 5 sec) was passed through the platinum-iridium recording pad of the probe one or two days prior to sacrificing the animals. The rats were deeply anesthetized and perfused through the heart first with 0.9% saline solution followed by 4% paraformaldehyde solution. The brains were sectioned by a Vibroslice at 60 µm in the coronal plane. Sections were mounted on slides, Nissl-stained, and cover-slipped. The tracks of the silicon probe shanks were reconstructed from multiple sections. The combination of these labeling and histological methods allowed for the post-mortem identification of the tracks and recording sites (Supplementary Fig 1).

Data Analysis

All analysis was performed using custom-written tools in Matlab (Mathworks). For the analysis in memory and non-memory tasks, we defined the trial start as the end time of nose-poking (normalized position 0), and the trial end as just before the start of reward consumption (position 1). Only correct trials are included in the principal analyses in this paper. For the 4-Hz and theta phase extraction, LFPs in PFC and CA1 were filtered with a Butterworth filter with pass-band range 2-5 Hz and 7-11 Hz, respectively. Instantaneous 4-Hz and theta phases were estimated by Hilbert transformation of the filtered signals. The velocity of the animal was computed by using a window of 0.04 of normalized position (~10 cm). The dip in velocity at positions 0.4-0.6 corresponds to the right or left turning of the rat at the T junction.

Phase modulation analysis. The phase modulation analysis is based on our previous work (Sirota et al., 2008). Briefly, the Rayleigh test was used for assessing uniformity. The statistics $Z=R^2/n$ (R: resultant length, n: sampling number), or variance-stabilized log(Z), is used for significance test (Fig 3A, 5B; Sirota et al., 2008). To identify conditional differences of phase modulation between predicting and non-predicting neurons, mean phase histograms were also computed (Fig. 5c). Peak-to-trough height of the phase histograms was used for the assessment of statistical significance (P<0.05; permutation test).

Gamma-trough-triggered average. Gamma-trough-triggered average (Figure 3B) was computed as follows. First, the LFPs were filtered in a 30-80 Hz frequency band. Next, the troughs of largest amplitude gamma wave in each cycle of 4-Hz or theta oscillations was detected. Using the gamma-trough times, the original (broad-band) LFP was averaged.

Overall mean firing rate. The mean firing rates of the task-active neurons in the memory task were: PFC pyramidal cells= 2.3 ± 2.5 Hz (mean + SD), interneurons 9.6 ± 8.8 Hz; VTA putative DA cells = 5.1 ± 6.0 Hz, GABAergic cells = 10.4 ± 13.0 Hz; CA1 pyramidal cells = 3.1 ± 3.3 Hz, interneurons = 18.3 ± 17.4 Hz.

Statistical tests

Permutation test. Permutation test was used to identify conditional differences in powers of 4-Hz, theta or gamma oscillations, and regions of the significant differences in the maze (Figs 1, 2, 3 and 5). Detailed information of this method is available in our previous papers (Fujisawa et al 2008). For each session, we computed the power spectra as a function of position, in memory and non-memory task (Fig. 1C and F). Powers at the specific frequency (f=3.5 Hz for 4-Hz oscillation, f=8.5 Hz for theta oscillation) in each condition (i.e. memory and non-memory task sessions; $\lambda_{momory}(x)$ and $\lambda_{non}(x)$) were computed as a function of position. The average and SE across sessions are shown in Fig. 1G. Next, the difference $D_0(x) = \lambda_{momory}(x) - \lambda_{non}(x)$ were computed. The memory/non-memory assignments to the labels of sessions were randomly

permuted, and the $\lambda(x)$s and the statistic $D_1(x)$ under the permuted labels were re-estimated. This process was repeated R times to obtain the statistic from the original data, $D_0(x)$, along with the statistic from resample data, $D_1(x),...,D_R(x)$. Using this resampled (shuffled) data set, pointwise p-value (5%) at each point was computed. To avoid multiple comparison issues, we also computed the global 5% bands.

Clopper-Pearson confidence intervals. Clopper-Pearson intervals were used for calculating binominal confidence intervals (Clopper and Pearson, 1934). For calculating Clopper-Pearson intervals, we used matlab statistics toolbox (binofit.m).

SUPPREMENTAL REFERENCES

Clopper, C. J., and Pearson, E. S. (1934) The Use of Confidence or Fiducial Limits Illustrated in the Case of the Binomial. Biometrika *26*, 404-413.

Fujisawa, S., Amarasingham, A., Harrison, M. T. and Buzsáki, G. (2008) Behavior-dependent short-term assembly dynamics in the medial prefrontal cortex. Nature Neurosci. *11*, 823-834.

Geisler, S. and Zahm, D. S. (2005) Afferents of the ventral tegmental area in the rat-anatomical substratum for integrative functions. J. Comp. Neurol. *490*, 270-294.

Geisler, S., Derst, C., Veh, R. W. and Zahm, D. S. (2007) Glutamatergic afferents of the ventral tegmental area in the rat. J. Neurosci. *27*, 5730-5743.

Isomura, Y., Sirota, A., Ozen, S., Montgomery, S., Mizuseki, K., Henze, D. A. and Buzsáki, G. (2006) Integration and segregation of activity in entorhinal-hippocampal subregions by neocortical slow oscillations. Neuron *52*, 871-82.

Jin, X. and Costa, R. M. (2010) Start/stop signals emerge in nigrostriatal circuits during sequence learning. Nature *466*, 457-462.

Kirk, I. J., Odie, S. D., Konopacki, J. and Bland, B. H.(1996) Evidence for differential control of posterior hypothalamic, supramammillary, and medial mammillary theta-related cellular discharge by ascending and descending pathways. J. Neurosci. 16, 5547-5554.

Mitra, P. P. and Bokil H. Observed brain dynamics. (Oxford University Press, 2008).

Pastalkova, E., Itskov, V., Amarasingham, A., and Buzsáki, G. (2008). Internally generated cell assembly sequences in the rat hippocampus. Science *321*, 1322-1327.

Paxinos, G. and Watson, C. The Rat Brain in stereotaxic coordinates, fourth edition (Academic Press, 1998).

Puryear, C. B., Kim, M. J. and Mizumori, S. J. (2010) Conjunctive encoding of movement and reward by ventral tegmental area neurons in the freely navigating rodent. Behav. Neurosci. *124*, 234-247.

Robinson, S., Smith, D. M., Mizumori, S. J. and Palmiter, R. D. (2004) Firing properties of dopamine neurons in freely moving dopamine-deficient mice: effects of dopamine receptor activation and anesthesia. Proc. Natl Acad. Sci. USA *101*, 13329-13334.

Roesch, M. R., Calu, D. J. and Schoenbaum G. (2007) Dopamine neurons encode the better option in rats deciding between differently delayed or sized rewards. Nature Neurosci. *10*, 1615-1624.

Schultz, W. (2006) Behavioral Theories and the Neurophysiology of Reward. Annu. Rev. Psychol. *57*, 87-115.

Sirota, A., Montgomery, S., Fujisawa, S., Isomura, Y., Zugaro, M. and Buzsáki, G. (2008) Entrainment of neocortical neurons and gamma oscillations by hippocampal theta rhythm. Neuron *60*, 683-697.

Steriade, M., McCormick, D. A. and Sejnowski, T. J. (1993)Thalamocortical oscillations in the sleeping and aroused brain. Science *262*, 679-685.

Vinck, M., van Wingerden, M., Womelsdorf, T., Fries, P., and Pennartz, C. M. (2010) The pairwise phase consistency: a bias-free measure of rhythmic neuronal synchronization. Neuroimage 51, 112-122.

Waelti, P., Dickinson, A. and Schultz, W. (2001) Dopamine responses comply with basic assumptions of formal learning theory. Nature 412, 43-48.